

## THE INFRARED EMISSION BANDS. I. CORRELATION STUDIES AND THE DEPENDENCE ON C/O RATIO

MARTIN COHEN,<sup>1,2</sup> LOU ALLAMANDOLA,<sup>1,3</sup> A. G. G. M. TIELENS,<sup>1,4</sup> JESSE BREGMAN,<sup>1</sup>  
 J. P. SIMPSON,<sup>1,5</sup> FRED C. WITTEBORN,<sup>1</sup> DIANE WOODEN,<sup>1</sup> AND DAVE RANK<sup>5</sup>

Received 1985 May 30; accepted 1985 September 17

### ABSTRACT

We present new airborne measurements of the unidentified (UIR) emission bands between 5 and 8  $\mu\text{m}$  in eight planetaries, eight locations in five reflection nebulae, and seven locations in four H II regions (including the Orion Bar). These data are compared with preexisting and new ground-based observations of the 3.3, 8.7, and 11.3  $\mu\text{m}$  bands. Good correlations are found between the strengths of all pairs of bands, including two newly established weak bands at 5.6 and 6.9  $\mu\text{m}$ . This leads to the conclusion that all seven UIR features form a "generic spectrum"; however, there are real variations in the relative strengths of the features among the sources.

The fraction of total, far-infrared luminosity radiated by a planetary in the strongest UIR feature at 7.7  $\mu\text{m}$  is strongly correlated with the nebular C/O ratio. This strongly suggests that hydrocarbons are the carriers of these features. The recent suggestion that polycyclic aromatic hydrocarbon-like species are the carriers of the bands is examined. Infrared observations of the UIR bands in planetary nebulae are important because the carriers, the molecular precursors of carbon grains, are formed in these nebulae. For the first time, therefore, we can probe directly the actual process of dust condensation in these objects.

*Subject headings:* infrared: spectra — interstellar: molecules — line identifications — nebulae: H II regions — nebulae: planetary — nebulae: reflection — interstellar molecules

### I. INTRODUCTION

The unidentified infrared (hereafter UIR) bands constitute a spectrum of emission features at 3.3, 6.2, 7.7, 8.7, and 11.3  $\mu\text{m}$  (Aitken 1981; Barlow 1983). They are detected in planetary nebulae (Russell, Soifer, and Willner 1977; Bregman *et al.* 1983; and references therein), reflection nebulae (Sellgren, Werner, and Dinerstein 1983), in H II regions (Russell, Soifer, and Merrill 1977), and even in external galaxies (e.g., Aitken and Roche 1984). Recently, mysterious near-infrared continuum emission has been discovered in reflection nebulae (Sellgren, Werner, and Dinerstein 1983), which may even extend from the mid-IR (Sellgren *et al.* 1985) to the far-red (Witt, Schild, and Kraiman 1984) and may be related to the UIR bands.

Due to the ubiquity of the bands, much interest has focused on potential emission mechanisms and on the nature of the materials that produce them. Although several models have been proposed, until recently none was very satisfactory. In brief, these models are as follows: (1) infrared fluorescence from UV-pumped, vibrationally excited, small molecules (e.g., CH<sub>4</sub>, H<sub>2</sub>O, NH<sub>3</sub>, CO) frozen on 0.1  $\mu\text{m}$ -sized grains at low ( $\sim 10$  K) temperatures (Allamandola, Greenberg, and Norman 1979, and references therein); (2) equilibrium thermal emission from small (0.01  $\mu\text{m}$ ) grains at 300 K, coated with an unspecified polymeric material (Dwek *et al.* 1980); (3) equilibrium thermal emission from characteristic groups on aromatic-like moieties, present at the surface of small carbon grains (Duley and Wil-

liams 1981); (4) nonequilibrium thermal emission from very small grains (0.001  $\mu\text{m}$ ) of unspecified composition that are temporarily heated to 1000 K by the absorption of individual UV photons (Sellgren 1984). Sellgren (1984) has suggested that the fourth model may also account for the infrared continuum emission in reflection nebulae. There are drawbacks with each model. Model 1 requires a multicomponent mantle that does not change composition under a wide variety of interstellar conditions. Models 2 and 3 require values for the infrared oscillator strength ( $f$ ) near unity. Typically,  $f$  varies from  $10^{-5}$  to  $10^{-3}$  for vibrational transitions. Model 4 relies on the uncertain assumption that a 10 Å-sized species can be treated as if it has bulk thermal and optical properties.

Extending the ideas of Duley and Williams (1981) and of Sellgren (1984), Leger and Puget (1984) suggested that the UIR bands arise not from grains, but from free polycyclic aromatic hydrocarbon molecules (hereafter PAHs), such as coronene. The good agreement between the wavelengths of the observed UIR features and the Raman spectrum of automobile soot (a mixture of PAHs and small carbon particles) supports this suggestion (Allamandola, Tielens, and Barker 1985a). In the interstellar medium, these molecules are likely to be ionized and the UIR bands are due to UV-pumped fluorescence from ions in highly vibrationally, possibly in electronically, excited states (Allamandola, Tielens, and Barker 1985a).

The PAH hypothesis seems promising in that infrared bands at 3.3, 6.2, and near 7.7  $\mu\text{m}$  are characteristic of a collection of aromatic species. Moreover, these species are the first steps in the process of condensation of carbon-dust particles which presumably takes place in the carbon-rich outflow, from planetary nebulae (Crawford, Tielens, and Allamandola 1985). They are also sufficiently stable to withstand the rigors of the interstellar medium. The abundance of PAHs (with respect to

<sup>1</sup> NASA/Ames Research Center.

<sup>2</sup> Radio Astronomy Laboratory, University of California, Berkeley.

<sup>3</sup> NRC-Senior Associate.

<sup>4</sup> Space Sciences Laboratory, University of California, Berkeley.

<sup>5</sup> Lick Observatory, University of California, Santa Cruz.

hydrogen) that is necessary to account for the observed band intensities is of order  $10^{-7}$  (Allamandola, Tielens, and Barker 1985a).

Nonetheless, there are some problems. Spectra of individual neutral molecules do not match the entire emission spectrum observed, either in frequency, profile, or relative band intensities. These difficulties have been taken to imply that the carriers are modified in the interstellar environment. They may be partially hydrogenated (Duley and Williams 1981); or they could be present as larger neutral molecules than the small species investigated in the laboratory (Leger and Puget 1984); or they are electronically excited, and ionized (Allamandola, Tielens, and Barker 1985a). It is presumed that such modifications would change somewhat the spectrum of the neutral parent molecule to one that is closer to the observed UIR spectrum.

Unfortunately, there are very few laboratory data in the literature on the spectroscopic properties of partially hydrogenated, electronically excited, ionized PAHs. Even without all the relevant laboratory data, however, infrared observations can test, and place constraints on, the collection of interstellar PAHs. For example, one expects a correlation of the 6.2 and 7.7  $\mu\text{m}$  band intensities basically because both these features arise primarily from C—C stretching motions and they are close enough in energy that the ratio of band strengths should be only mildly dependent on the excitation mechanism. Further, these two UIR bands, the observations of which necessitate airborne observations, lie in the richest and most intense region of the spectrum of PAHs (since all the C—C stretching modes of these carbon-rich hydrocarbons fall in this spectral range). Finally, one would hope to find a quantitative dependence of band strength on carbon richness of the environment in which these hydrocarbons are manufactured. The crucial aspect of the planetary nebulae is that, as a class, they are objects in which the materials that produce the UIR features are created, unlike reflection nebulae, where these materials probably antedate the young hot stars that now illuminate diffuse interstellar clouds. A quantitative dependence of the presence of UIR bands on C/O ratio in planetaries was demonstrated by Barlow (1983, his Table 4).

This paper is organized as follows. Sections II and III describe the observations and the determination of the strengths of the UIR features. In § IV, the correlations between these features are examined, while in § V the dependence on nebular C/O ratio is investigated. In § VI, the results are discussed with the emphasis on the PAH hypothesis.

## II. THE OBSERVATIONS

All our airborne observations were taken from the Kuiper Airborne Observatory, from an elevation of 41,000 feet, using the 24 detector, liquid helium-cooled Faint Object Grating Spectrograph (FOGS; Witteborn and Bregman 1984). The 24 Si:Bi detectors (23 of which operated) were multiplexed so that each was integrating essentially all the time. The signal level on each one was sampled several times during each extreme of the secondary mirror motion. The signals were digitized and stored in 24 element arrays by a computer on disk memory. The resolution of the FOGS was 0.12  $\mu\text{m}$  per channel (or detector,  $\lambda/\Delta\lambda \approx 50$ ) in the configuration used for the KAO flights. Wavelength calibration was performed by internal observations of a blackbody through a polystyrene sheet that yields deep absorptions at known wavelengths. Flux calibration and removal of telluric absorptions was achieved by

observations of standard stars ( $\beta$  And,  $\alpha$  Tau,  $\beta$  Gem, and  $\alpha$  Leo) with known photospheric temperatures. Wavelength coverage was from 5.27 to 8.09  $\mu\text{m}$  with  $\Delta\lambda = 0.12 \mu\text{m}$ . Typical observations involved between 25 and 45 minutes of integration on each source. Aperture size was 21" FWHM.

Table 1 presents a journal of the airborne observations that includes dates and the actual integration time employed for all relevant planetaries, reflection nebulae, and H II regions. Figure 1 shows all our KAO spectra of the planetaries and of M1-78 and of GL 437, both of which are H II regions. The observations of Orion and of the reflection nebula P18 will be discussed in detail elsewhere. In addition, we have made observations of the 3.3  $\mu\text{m}$  feature in the Orion Bar region using 5".4 FWHM apertures with the seven detector Cooled Grating Spectrometer (Wade 1983) at the UKIRT in 1984 December (Bregman *et al.* 1985). We have also measured the 8.7 and 11.3  $\mu\text{m}$  features in the Orion Bar and at several positions around P18 with the FOGS at Mount Lemmon in 1985 February (approximately 9" FWHM beams).

## III. UIR BAND STRENGTHS

For each nebula we defined the continuum through the airborne observing region by a smooth interpolation between

TABLE 1  
JOURNAL OF AIRBORNE OBSERVATIONS

Object	Nebular Type <sup>a</sup>	Position <sup>b</sup>	Date	Integration (minutes)
NGC 7023 .....	RN	20°N, 30°W	1983 Nov 29	58
Orion Bar .....	H II	position 4	1983 Nov 29	52
HD 44179 .....	RN	star	1983 Nov 29	16
GL 437 .....	H II	GL 437W	1983 Nov 29	34
NGC 7023 .....	RN	20°N, 30°W	1983 Dec 1	22
Orion Bar .....	H II	position 4	1983 Dec 1	9
	H II	10°S	1983 Dec 1	9
	H II	20°S	1983 Dec 1	9
	H II	10°N	1983 Dec 1	9
M1-11 .....	PN	...	1983 Dec 1	14
IC 5117 .....	PN	...	1983 Dec 2	30
NGC 2023 .....	RN	60°S	1983 Dec 2	47
Orion Bar .....	H II	10°N	1983 Dec 2	6
	H II	20°S	1983 Dec 2	10
M1-11 .....	PN	...	1983 Dec 2	18
NGC 6790 .....	PN	...	1984 Jul 19	26
SAO 161375 .....	H II	star	1984 Jul 19	26
NGC 6572 .....	PN	...	1984 Jul 19	32
M1-78 .....	H II	...	1984 Jul 19	30
BD + 30°3639 .....	PN	...	1984 Jul 19	20
NGC 6790 .....	PN	...	1984 Jul 24	26
SAO 161375 .....	H II	star	1984 Jul 24	20
NGC 6572 .....	PN	...	1984 Jul 24	30
M1-78 .....	H II	...	1984 Jul 24	24
BD + 30°3639 .....	PN	...	1984 Jul 24	12
IC 418 .....	PN	...	1985 Jan 26	24
M4-18 .....	PN	...	1985 Jan 26	29
Parsamian 18 .....	RN	12°N, 12°W	1985 Jan 26	29
NGC 2071 .....	RN	30°N, 30°E	1985 Jan 29	24
Parsamian 18 .....	RN	12°N	1985 Jan 29	32
		15°W	1985 Jan 29	28
NGC 2071 .....	RN	30°S, 20°E	1985 Feb 1	36
J900 .....	PN	...	1985 Feb 1	42

<sup>a</sup> Nebulae are either planetaries (PN), H II regions (H II), or reflection nebulae (RN).

<sup>b</sup> Positions designate the locations in reflection nebulae with respect to the following stars: HD 200775 (NGC 7023); HD 37903 (NGC 2023); "P18" (NE star at apex of fan nebula, Parsamian 18); HD 38563 (NGC 2071). For the Orion Bar, "position 4" is as defined by Becklin *et al.* 1976, and other locations are relative to position 4.

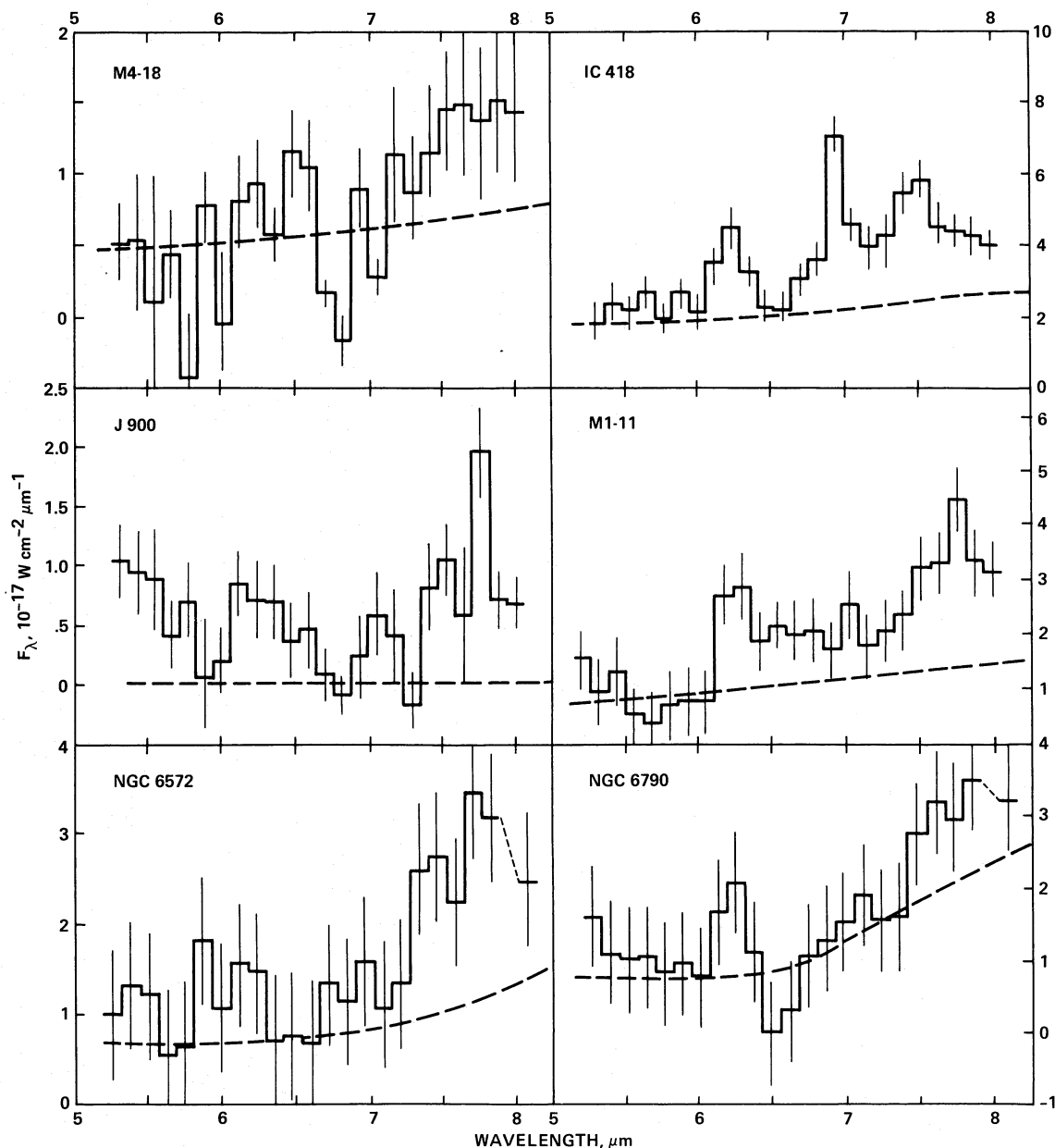


FIG. 1.—Airborne spectra of planetary nebulae, M1-78 and GL 437. Ordinate is  $F_{\lambda}$  in units of  $10^{-17} \text{ W cm}^{-2} \mu\text{m}^{-1}$ ; abscissa is wavelength, in  $\mu\text{m}$ . Dashed lines represent the interpolated continua used to define integrated band intensities. Average photometric error bars are shown.

ground-based broadband measurements at  $3.6$  or  $4.8 \mu\text{m}$  and a variety of ground-based data in the  $10 \mu\text{m}$  region. We used one, or more, of several techniques to define the relevant continuum levels at long wavelengths. These methods in order of decreasing desirability, were based on the following data: (1) a detailed spectrum ( $\Delta\lambda/\lambda \approx 0.02$ ) through an aperture either comparable with our KAO beam for extended objects, or at least much larger than the nebular size for very small objects; (2) a detailed spectrum, through an aperture different from our own but that could be scaled by the overlap of the airborne and ground-based data near  $8.0 \mu\text{m}$ ; (3) a narrow-band filter ( $\Delta\lambda/\lambda \leq 0.1$ ) measurement at  $\sim 9.8 \mu\text{m}$ , a wavelength that is uncontaminated by emission lines or bands (cf. Cohen and Barlow 1980); (4) a narrow-band filter observation at  $10.8 \mu\text{m}$  (we rejected data at  $8.6$  and  $11.3 \mu\text{m}$  because both these filters are contami-

nated by broad emission features); and (5) an interpolation between apparent flux minima near  $5.5$ – $5.9$  and  $6.5$ – $6.8 \mu\text{m}$ .

Method 1, the most reliable, was available for J900 and NGC 7027. Method 2, which we estimate to be only slightly less valuable than method 1, was used for M4-18, IC 418, M1-11, NGC 6572, NGC 6790, BD +30°3639, IC 5117, NGC 2023 and 7023, HD 44179, GL 437, the four (airborne) Orion Bar locations, and M1-78. Method 3 was not used alone but did provide general corroboration of the continuum flux level (obtained by method 2) of IC 418 at  $9.8 \mu\text{m}$ . Likewise, method 4 was used to check the levels (obtained by method 2) for NGC 6790, IC 5117, and M1-78. Method 5, although attended by some uncertainty, was the only technique at our disposal for the following objects: NGC 2071, P18, and SAO 161375. The uncertainties that result in the interpolated continua from any

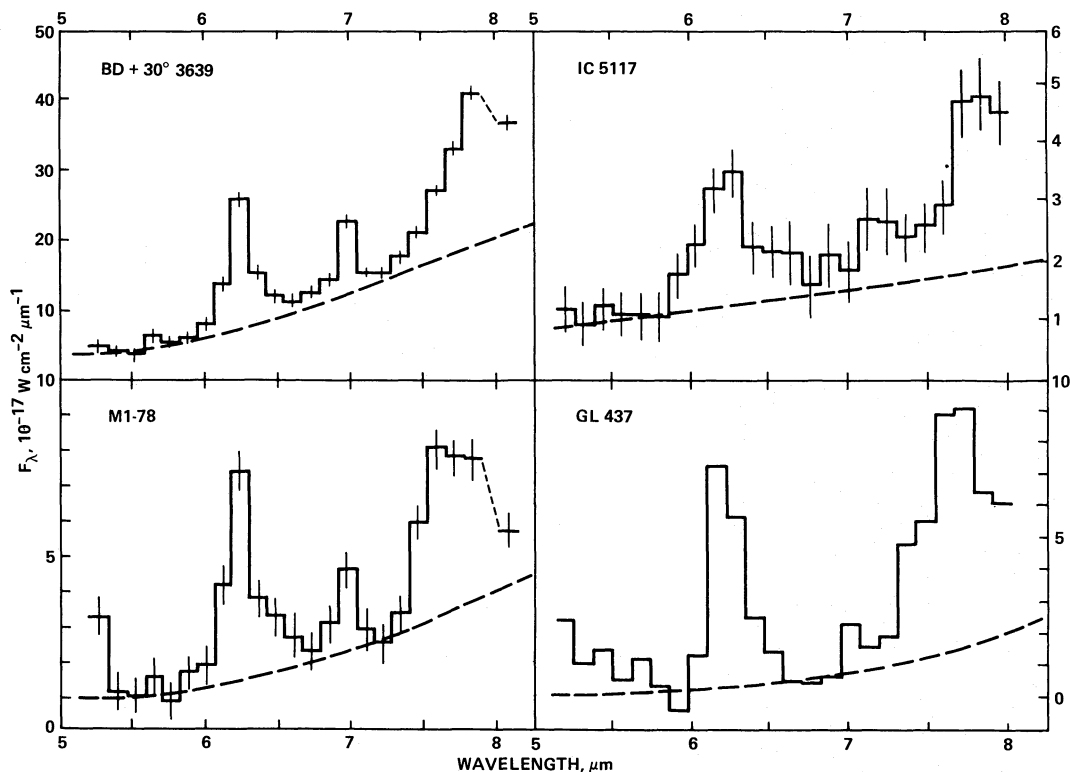


FIG. 1.—Continued

of these methods are less at  $6.2 \mu\text{m}$  (which is relatively close to the data at  $3.6$  or  $4.8 \mu\text{m}$ ) than at  $7.7 \mu\text{m}$ . However, the continuum uncertainties even at  $7.7 \mu\text{m}$  are diminished somewhat by the partial dependence on the short-wavelength fluxes, which lessens the effects of errors in flux level at  $\sim 10 \mu\text{m}$ . For example, even a 50% error in flux level at  $9.8 \mu\text{m}$  would lead to an error of only 25% in integrated intensity of the  $7.7 \mu\text{m}$  feature and would have almost negligible effect ( $\leq 5\%$ ) on that at  $6.2 \mu\text{m}$ , where the estimates of flux are based on any of methods 1–4. It is much harder to assess the errors implicit in method 5. This method will always yield an underestimate for the intensities of the  $6.2$  and  $7.7 \mu\text{m}$  features since it ignores any underlying continuum (or “plateau” of emission) below these bands. After our initial estimates of these band strengths in P18 we obtained some (smaller aperture)  $8$ – $13 \mu\text{m}$  spectra at the three different locations, albeit with rather poor signal-to-noise ratios. These spectra suggested that the intensity of the  $7.7 \mu\text{m}$  feature might even be double our original estimate, while the  $6.2 \mu\text{m}$  band could be increased by  $\sim 35\%$ . However, P18, like the Orion Bar, is a source in which we can make a strong case for the existence of a broad emission plateau underlying the strong discrete features. We shall defer a more detailed discussion of both the Orion Bar region (Bregman *et al.* 1985) and P18 to subsequent papers. The chosen continua are shown in Figure 1.

We defined the wavelength limits of the strong  $6.2$  and  $7.7 \mu\text{m}$  bands from our observations of HD 44179 (see Fig. 2 for its composite spectrum) and BD +  $30^\circ 3639$  (Fig. 1). These indicate that the maximum extent of the “ $6.2 \mu\text{m}$ ” feature is  $6.0$ – $6.6 \mu\text{m}$ . The intensity of the  $6.2 \mu\text{m}$  band was taken to be the flux, above the interpolated continuum, integrated between these limits. Some objects show clear wings to this feature (for example, IC 5117 and HD 44179). This wing is generally

included in the strength estimates. There is some evidence for this wing in the previously published CVF spectrum of HD 44179 (Russell, Soifer, and Willner 1978). The higher signal-to-noise ratio in the FOGS spectrum illustrates the advantages inherent in a multidetector spectrometer. For the  $7.7 \mu\text{m}$  band we augmented our  $5$ – $8 \mu\text{m}$  data by ground-based measurements which show that the “ $7.7 \mu\text{m}$ ” band is nearly symmetric, once the contribution of the  $8.7 \mu\text{m}$  feature is removed. It originates near  $7.3 \mu\text{m}$  and peaks between  $7.6$  and  $7.8 \mu\text{m}$ . Therefore the intensity of the  $7.7 \mu\text{m}$  feature was calculated as twice the integrated flux above continuum between  $7.4 \mu\text{m}$  and

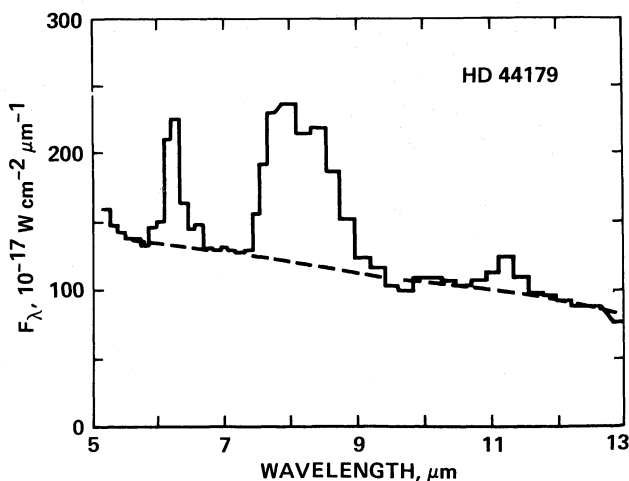


FIG. 2.—Composite spectrum of HD 44179 showing the symmetry of the  $7.7 \mu\text{m}$  feature. The  $5$ – $8 \mu\text{m}$  spectrum was taken with the FOGS on the KAO; the  $8$ – $13 \mu\text{m}$  spectrum was taken with the FOGS on Mount Lemmon.

the wavelength of the peak, corrected for the contribution of  $Pf\alpha$  and  $H\beta$ . This later correction was estimated from continuum radio fluxes (in Jy) by the relation  $I(Pf\alpha) = (6.65E - 19/8.70E - 19/1.15E - 18)S_{\nu}(5 \text{ GHz}) \text{ W cm}^{-2}$ , where the three multipliers are appropriate for  $n_e \approx 10^4 \text{ cm}^{-3}$ , case B recombination, and  $T_e = 5000/10,000/20,000 \text{ K}$ , respectively. ( $T_e$  was taken from Pottasch 1984, his Appendix 1.)

This treatment does not take into account the broad underlying "hump", starting near  $5.5 \mu\text{m}$ , peaking near  $8 \mu\text{m}$  and ending at about  $9.6 \mu\text{m}$  that is evident in some spectra such as that of the Orion Bar, NGC 7027, and NGC 7023 and 2023 (Bregman *et al.* 1985; Russell, Soifer, and Willner 1977; Sellgren *et al.* 1985). Our integrated band strengths, for all features, refer solely to the well-defined "sharper" spectral structures at the key wavelengths. Since this "hump" is not present in all of the spectra (compare HD 44179 with NGC 7027), it probably represents a separate component of both the emission spectrum and carriers.

In several spectra we found clear evidence for the two weaker unidentified features at  $5.6$  and  $6.9 \mu\text{m}$  that were recently attributed to the UIR spectrum by Bregman *et al.* (1983).

Their presence in the spectra of reflection nebulae rules out an origin in ionic lines. The first is very sharp (not more than  $0.12 \mu\text{m}$  FWZI). The latter is somewhat broader, spanning the range  $6.85\text{--}7.1 \mu\text{m}$  approximately (depending on the object), and is therefore distinguishable from the narrow  $6.99 \mu\text{m}$  Ar II line (e.g., see M1-78, Fig. 1). The nature of these new emission features will be discussed elsewhere (Allamandola, Tielens, and Barker 1985b). Assembled in Table 2 are the integrated band strengths for all four of these features that are observable solely from the air. To facilitate intercomparisons between these bands and those observed from the ground, we include in Table 2 band strengths for the  $3.3$ ,  $8.7$ , and  $11.3 \mu\text{m}$  features from our own data and from the literature, too. We have attempted to rationalize the method of integration by returning to the original observations of these bands in the various objects and using identical criteria to define the continua, UIR band widths and wavelength limits for the features in each object, rather than merely accepting band intensities from the literature. This should eliminate those discrepancies and inconsistencies in strengths that can arise when different sets of authors analyze similar data by different schemes. We have

TABLE 2  
OBSERVED, INTEGRATED BAND STRENGTHS FOR OBJECTS

OBJECT	POSITION	UIR BAND ( $\mu\text{m}$ )							References
		3.3	5.6	6.2	6.9	7.7	8.7	11.3	
Planetary									
M4-18	...	...	...	<0.8	...	<0.35	0.76	1.6	1
IC 418	...	1.8	1.0	5.9	2.4	14	...	8.0	2, 3
J900	...	0.36	...	3.2	...	7.5	0.82	0.72	1, 4
M1-11	...	0.31	0.6	7.2	<0.8	18	1.0	1.4	1, 5
NGC 6572	...	0.47	...	<2.2	...	12	...	<0.7	1, 6
NGC 6790	...	...	...	3.2	...	8.0	<0.7	<1.3	3
BD +30°3639	...	6.4	3.0	49	6.0	120	5.6	11	1, 2
NGC 7027	...	31	<84 <sup>a</sup>	120	12	520	28	165	7
IC 5117	...	0.84	0.2:	11	0.6	9.8	1.3	4.0	1, 4
Reflection Nebulae									
NGC 2023	60°S	0.76	1.1	4.1	1.8	8.6	...	...	8
NGC 2071	30°N, 30°E	...	2.8	9.6	2.5	18	...	...	...
	30°S, 30°E	...	1.2	5.7	1.1	9.9	...	...	...
HD 44179	...	74	<2.7	320	<2.7	600	110	150	2
P18	12°N, 12°W	...	0.39	9.6	0.50	9.7	<2.1	<1.3	9
	12°N	...	2.7	37	10	40	<0.8	<2.7	9
	15°W	...	5.5	51	3.9	67	2.5	2.6	9
NGC 7023	20°N, 30°W	0.86	1.4	14	4.1	12	...	...	8
H II Regions									
GL 437	GL 437W	2.7	1.3	19	0.7	37	33	22	10
Orion Bar	position 4	0.99	9.6	40	<8.4	77	2.7	10	4, 9
	5°N	0.41	...	...	...	...	1.9	6.5	4, 9
	10°N	0.23	3.6	22	<6.0	55	2.5	2.5	4, 9
	5°S	0.80	...	...	...	...	4.8	11	4, 9
	10°S	0.48	6.0	48	<4.8	67	3.3	5.0	4, 9
	15°S	0.40	...	...	...	...	3.1	4.8	4, 9
	20°S	0.29	3.0	28	3.2	36	2.5	2.7	4, 9
SAO 161375	...	...	<1.2	33	6.0	92	...	...	...
M1-78	...	1.7	0.48	11	0.72	26	...	4.8	1, 4

NOTE.—Entries ordered by R.A. within nebular types. UIR bands designated by their central wavelengths in  $\mu\text{m}$ . Strengths in units of  $10^{-18} \text{ W cm}^{-2}$ .

<sup>a</sup> NGC 7027's  $5.6 \mu\text{m}$  UIR band is contaminated, to an unknown extent, by its [Mg v] emission line.

REFERENCES.—(1) Aitken and Roche 1982. (2) Russell, Soifer, and Merrill 1977. (3) Aitken *et al.* 1979. (4) Unpublished  $3.3 \mu\text{m}$  measurements from UKIRT, 1984 December, by Geballe, Allamandola, and Tielens (Bregman *et al.* 1985). (5) Allen *et al.* 1982. (6) Willner *et al.* 1979. (7) Bregman *et al.* 1983. (8) Sellgren *et al.* 1983; Sellgren *et al.* 1985. (9) Unpublished  $8.7$  and  $11.3 \mu\text{m}$  observations from Mount Lemmon, 1985 February, by Bregman. (10) Kleinmann *et al.* 1977.

also kept track of the relative sizes of objects and the aperture used for observations of different bands so that comparisons between ground-based and airborne bands can be made either with effectively identical apertures or with apertures that encompass nebulae in their entirety. We applied aperture corrections to the following nebulae to scale up the small-aperture 8–13  $\mu\text{m}$  observations to our KAO (21") data: NGC 6572, NGC 6790, BD +30°3639, GL 437, the various positions in the Orion Bar region, and in Parsamian 18. For GL 437, the growth of at least the broad-band signal with aperture was established by Kleinmann *et al.* (1977). For all other nebulae the scaling factor was determined by comparing the longest wavelength flux (that at 8.1  $\mu\text{m}$ ) in our airborne spectra with the shortest wavelength ground-based measurement (usually at 8.1 or 8.2  $\mu\text{m}$ ).

To seek a correlation of the 3.3 and 11.3  $\mu\text{m}$  features it was further necessary to scale our new 3.3  $\mu\text{m}$  data (with 5"4 beams) to those between 8 and 13  $\mu\text{m}$  (with approximately 9" beams) of the Orion Bar. We achieved this scaling by investigation of that necessary to scale up the continuum for "position 4" of the Bar, defined with 4"5 apertures by Becklin *et al.* (1976) at 9.5, 11.2, and 12.5  $\mu\text{m}$ , to our Mount Lemmon data (9" beams).

This comparison suggested that we scale up the 3.3  $\mu\text{m}$  band luminosities by a factor of 3.4 in going from UKIRT to the Mount Lemmon beams.

Note that Table 2 reports strictly the observed band intensities, uncorrected for beam-size effects, but corrected for the contributions of Pf $\delta$  to the 3.3  $\mu\text{m}$  band flux, according to the relation  $I(\text{Pf}\delta) = 4.22E-19/2.43E-19/1.53E-19S_\nu(5 \text{ GHz}) \text{ W cm}^{-2}$  that relates the line strength to the radio recombination continuum (in Jy) at 5 GHz for the planetaries whose radio fluxes are known. Aperture corrections are, however, incorporated into Table 3 which is described below.

#### IV. CORRELATIONS BETWEEN UIR BANDS

In our correlation study of the UIR features we have compared the following bands, pairwise: 6.2 and 7.7  $\mu\text{m}$ ; 6.9 and 6.2  $\mu\text{m}$ ; 5.6 and 7.7  $\mu\text{m}$ ; 5.6 and 6.9  $\mu\text{m}$ ; 11.3 and 3.3  $\mu\text{m}$ ; 11.3 and 7.7  $\mu\text{m}$ ; and 11.3 and 5.6  $\mu\text{m}$  (Figs. 3–9, respectively). To give a sense of the intrinsic strengths of these features from object to object we have chosen to convert the observed strengths (Table 2) into band luminosities. These luminosities are used in Figures 3–9, together with the distance indicated in Table 3, that summarizes these luminosities.

TABLE 3  
INTRINSIC BAND LUMINOSITIES (IN  $L_\odot$ )

OBJECT	POSITION	UIR BAND ( $\mu\text{m}$ )							DISTANCE (kpc)	REFERENCES	
		3.3	5.6	6.2	6.9	7.7	8.7	11.3			
Planetaries											
M4-18	...	...	...	<0.25	...	1.1	0.23	...	0.48	1	1
IC 418	...	0.07	0.04	0.23	0.10	0.57	...	...	0.32	0.36	2
J900	...	0.56	...	5.0	...	12	1.3	...	1.1	2.25	2
M1-11	...	0.10	0.18	2.2	<0.25	5.5	0.31	...	0.42	1	1
NGC 6572	...	0.07	...	<0.30	...	1.6	...	...	<0.22	0.67	2
NGC 6790	...	...	...	2.5	...	6.3	<1.6	...	<3.0	1.6	2
BD +30°3639	...	0.83	0.39	6.4	0.78	16	1.1	...	2.2	0.65	2
NGC 7027	...	11	31	44	4.4	190	10	...	60	1.1	2
IC 5117	...	1.3	<0.36	16	0.89	14	2.0	...	6.0	2.2	2
Reflection Nebulae											
NGC 2023	60°S	0.05	0.07	0.27	0.12	0.56	...	...	...	0.46	3
NGC 2071	30°N, 30°E	...	0.18	0.62	0.16	1.18	...	...	...	0.46	3
	30°S, 30°E	...	0.08	0.37	0.07	0.65	...	...	...	0.46	3
HD 44179	...	1.8	<0.09	7.8	<0.09	15	2.7	...	3.6	0.28	4
P18	12°N, 12°W	...	0.14	3.6	0.18	3.6	<11	...	<6.7	1.1	5
	12°N	...	1.0	14	3.8	15	<1.7	...	<5.7	1.1	5
	15°W	...	2.1	19	1.4	25	10	...	11	1.1	5
NGC 7023	20°N, 30°W	0.51	0.09	0.82	0.24	0.72	...	...	...	0.44	6
H II Regions											
GL 437	GL 437W	7.5	3.7	52	2.0	100	92	...	62	3.0	7
Orion Bar	Position 4	0.22 <sup>a</sup>	0.63	2.6	<0.55	5.0	0.18/0.74 <sup>b</sup>	...	0.66/2.7 <sup>b</sup>	0.46	3
	5°N	0.09	...	...	...	...	0.12/	...	0.42/	0.46	3
	10°N	0.05	0.23	1.4	<0.40	3.6	0.16/1.0	...	0.16/1.0	0.46	3
	5°S	0.18	...	...	...	...	0.31/	...	0.72	0.46	3
	10°S	0.11	0.40	3.1	<0.31	4.4	0.22/1.6	...	0.33/2.4	0.46	3
	15°S	0.09	...	...	...	...	0.20/	...	0.31/	0.46	3
	20°S	0.07	0.20	1.8	0.21	2.4	0.16/1.3	...	0.18/1.4	0.46	3
SAO 161375	...	...	<2.1	58	11	160	...	...	...	2.4	8
M1-78	...	9.8	2.9	67	4.3	160	...	...	29	4.4	2

NOTE.—All luminosities are directly comparable (aperture-corrected) except for those of the Orion Bar.

<sup>a</sup> All luminosities at 3.3  $\mu\text{m}$ , for the Orion Bar, are scaled up to the aperture of the 11.3  $\mu\text{m}$  Mount Lemmon observations and are directly comparable to the first numbers in the 8.7 and 11.3  $\mu\text{m}$  Orion Bar columns.

<sup>b</sup> First entries at 8.7 and 11.3  $\mu\text{m}$ , for the Orion Bar, are comparable directly with those at 3.3  $\mu\text{m}$ . Second entries are scaled, by the continua, for direct comparison with the larger aperture KAO measurements of the Orion Bar.

REFERENCES.—(1) Adopted as 1 kpc. (2) Acker 1978. (3) 460 pc taken for all Orion sources. (4) Schmidt, Cohen, and Margon 1980. (5) From unpublished optical spectroscopy by Cohen. (6) Whitcomb *et al.* 1981. (7) Wynn-Williams *et al.* 1981. (8) Taken to be at the distance of M17.

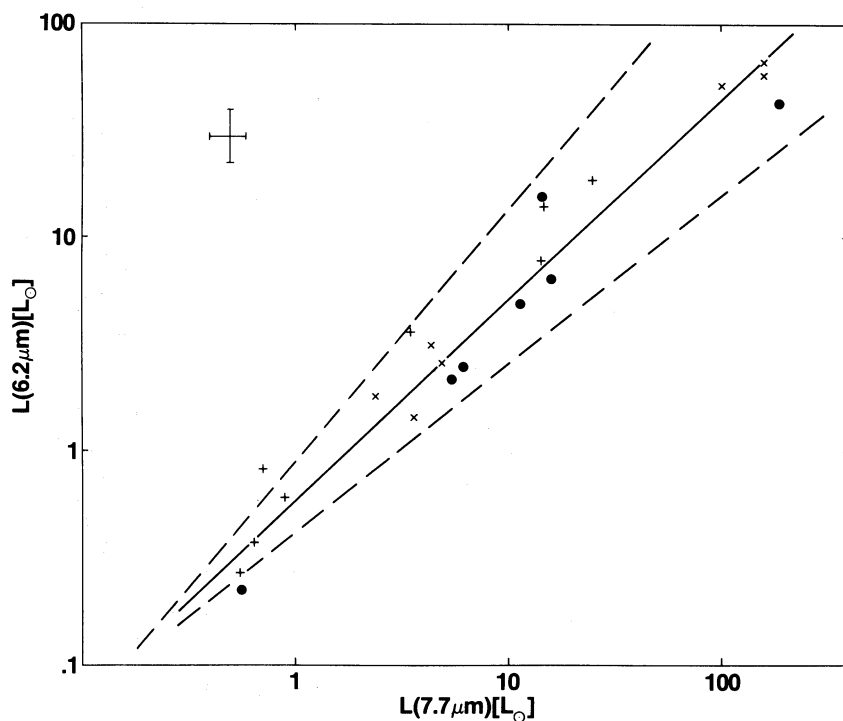


FIG. 3.—Correlation between 7.7 and 6.2  $\mu\text{m}$  UIR band luminosities. Symbols are *filled circles*, planetary nebulae; *crosses*, H II regions, or locations in these; *plus signs*, reflection nebulae, or locations in these. The asymmetric large cross in the upper left represents typical error bars for the two band strengths. Solid line is the best-fit line; dashed lines, flanking this, are defined from the formal variances in the  $\chi^2$  fitting procedures for slope and intercept.

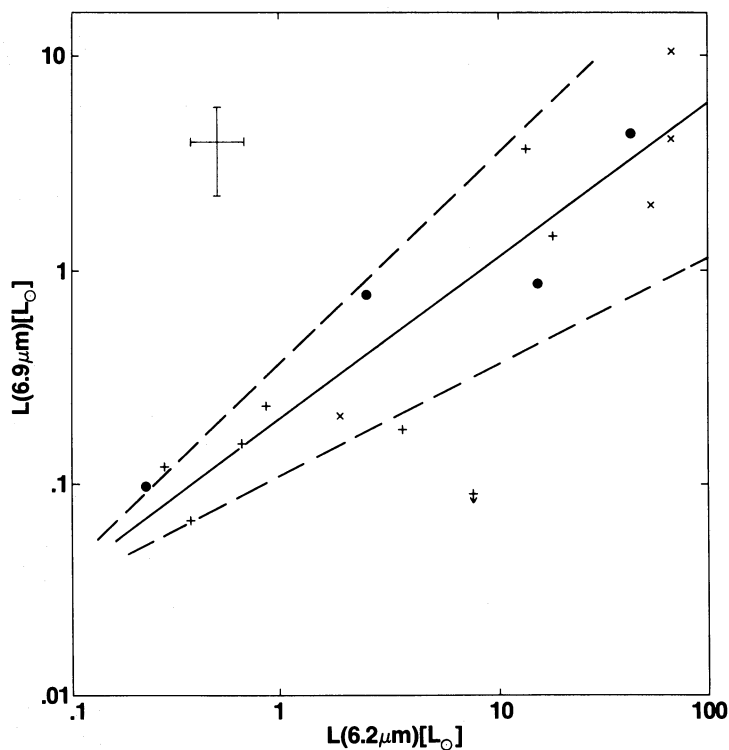


FIG. 4.—Correlation between 6.9 and 6.2  $\mu\text{m}$  UIR bands. Symbols and structure as for Fig. 3. The solitary upper limit, plotted below the correlation lines, represents HD 44179. This limit was not incorporated into the fitting procedure.

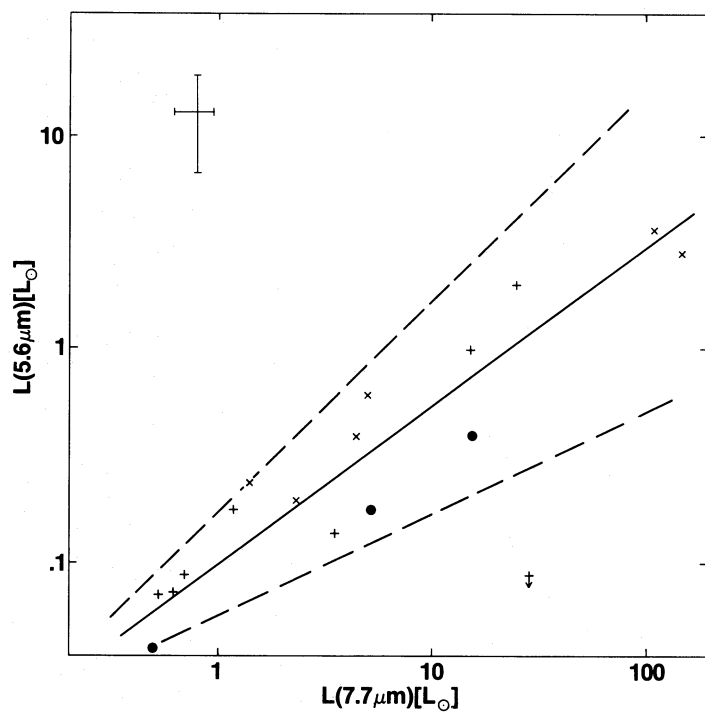


FIG. 5.—Correlation between 5.6 and 7.7  $\mu\text{m}$  UIR bands. Details as for Fig. 3. The upper limit is for HD 44179.

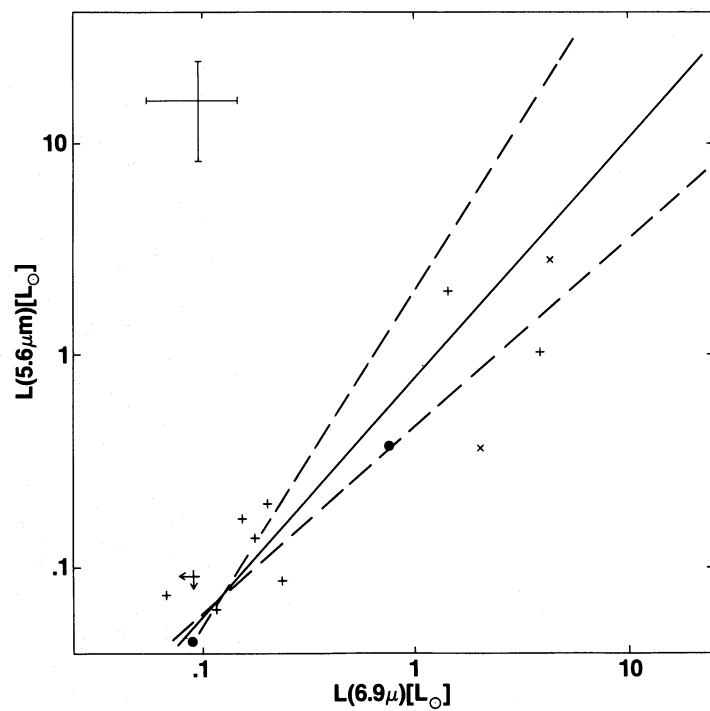


FIG. 6.—Correlation between the two new weak bands at 5.6 and 6.9  $\mu\text{m}$ . Details as for Fig. 3. Double limit is for HD 44179.

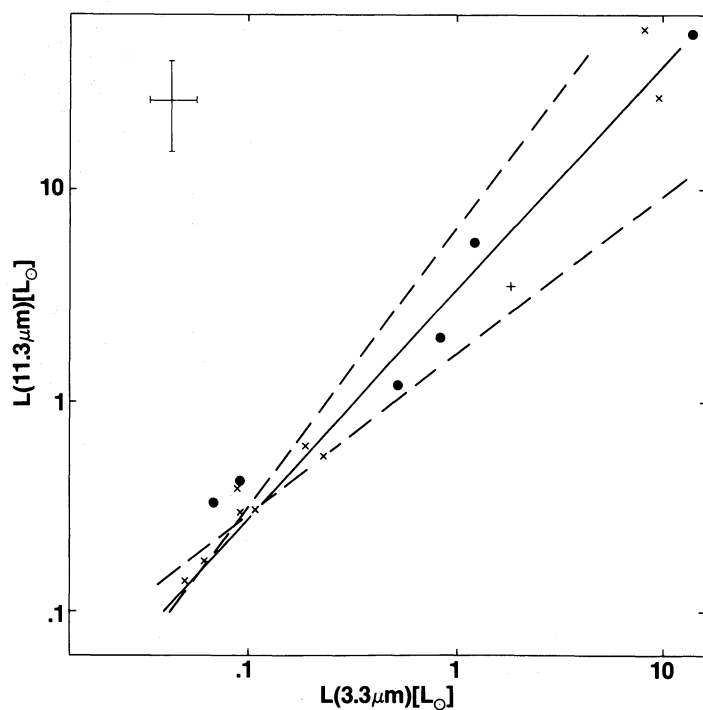


FIG. 7.—Correlation between the strongest UIR features visible from the ground, at 11.3 and 3.3  $\mu\text{m}$ . Details as for Fig. 3.

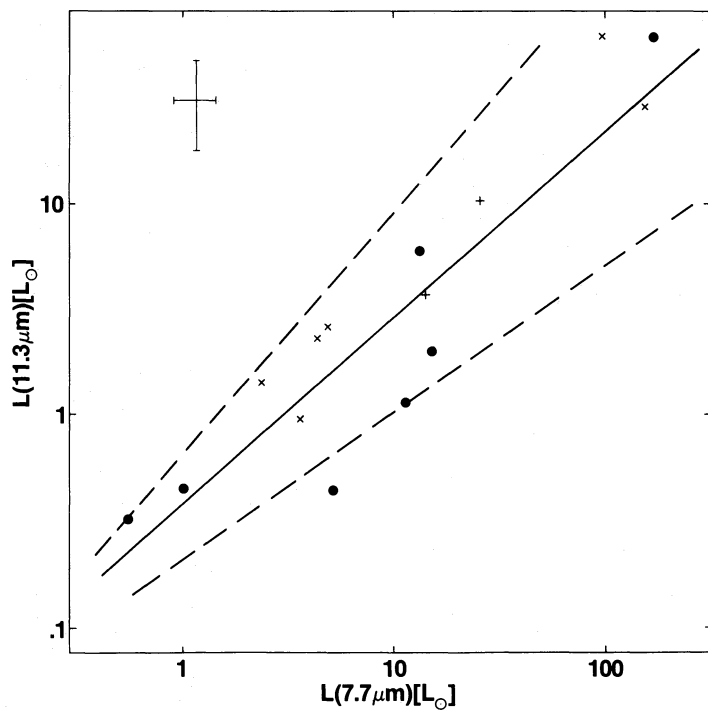


FIG. 8.—Correlation between UIR bands at 11.3 and 7.7  $\mu\text{m}$ . Details as for Fig. 3.

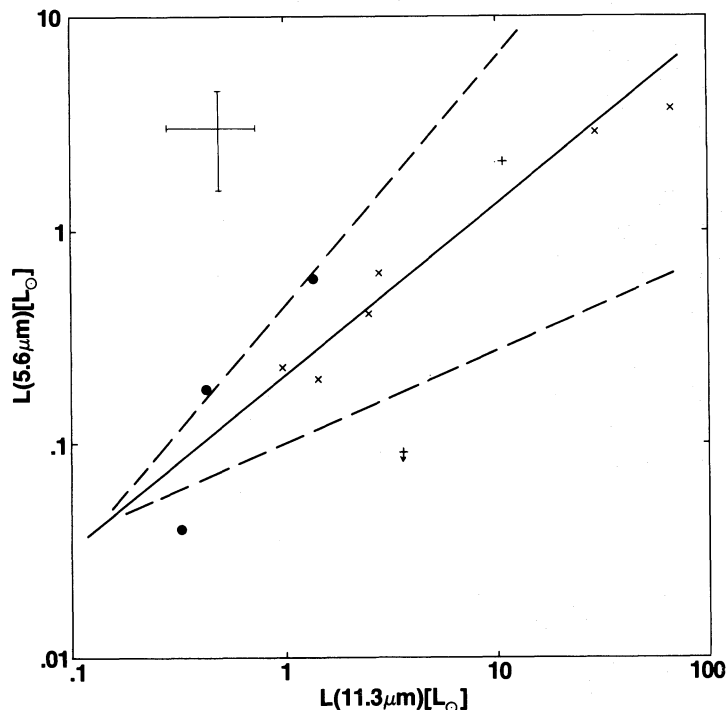


FIG. 9.—Correlation between UIR bands at 11.3 and 5.6  $\mu\text{m}$ . Details as for Fig. 3. Upper limit is for HD 44179.

Figures 3–9 present definite trends, the analysis of which we now discuss. The significance of all these potential correlations is high; values of  $r^2$  (the correlation coefficient, defined as  $[\Sigma xy - (\Sigma x \Sigma y / N)]^2 / [\Sigma x^2 - (\Sigma x)^2 / N][\Sigma y^2 - (\Sigma y)^2 / N]$ ) range from 0.82 to 0.95 (see Table 4). To quantify these relationships we have used  $\chi^2$  methods to fit the best line to the (log, log) plots of band strengths. Table 4 summarizes the best fit slopes and intercepts, together with their standard error estimates (defined from the half-range over which  $\chi^2$  increases by 1). In Figures 3–9 we show the mean lines and the 1 standard error lines, defined as the lines that have the lowest values of slope and intercept, and the highest values, for each correlation. To compare these lines with the actual observed band luminosities we have included error bars in each figure that characterize the typical (as represented by IC 418) uncertainties in band strengths, assessed from the combination of uncertainties in underlying continuum levels and those due to photometric statistics in each spectrometer channel.

The values of mean slopes (Table 4) are all close to unity. In

TABLE 4  
CORRELATIONS BETWEEN BAND STRENGTHS  
( $\text{LOG } I_1 = \text{SLOPE} * \text{LOG } I_2 + \text{INTERCEPT}$ )

$\lambda_1$	$\lambda_2$	Slope ( $\pm 1 \sigma$ )	Intercept ( $\pm 1 \sigma$ ) <sup>a</sup>	Correlation Coefficient ( $r^2$ )
7.7.....	6.2	$1.05 \pm 0.22$	$0.25 \pm 0.21$	0.95
6.9.....	6.2	$0.73 \pm 0.23$	$-0.68 \pm 0.26$	0.88
5.6.....	7.7	$0.73 \pm 0.25$	$-1.00 \pm 0.24$	0.95
6.9.....	5.6	$0.88 \pm 0.25$	$0.08 \pm 0.29$	0.86
11.3.....	3.3	$1.04 \pm 0.32$	$0.57 \pm 0.30$	0.95
11.3.....	7.7	$0.92 \pm 0.21$	$-0.44 \pm 0.26$	0.82
5.6.....	11.3	$0.80 \pm 0.37$	$-0.67 \pm 0.32$	0.91

<sup>a</sup> Formal error in  $\chi^2$ -fitting, corresponding to the interval over which  $\chi^2$  increases by 1 over its minimum value.

fact, the intersection of all six ranges for slope is the interval  $0.90 \pm 0.06$ , and the  $1/\sigma^2$ -weighted average of the mean slopes is 1.02. This suggests that the band strengths are all essentially linearly correlated with one another. From the intercepts in Table 4 we derive the average ratios of bands expressed by the correlations. This enables us to determine a “generic spectrum” that represents each band by its average strength relative to the strongest band, that at 7.7  $\mu\text{m}$ . Figure 10 and Table 5 show this generic spectrum. The general correlation of the 5.6 and 6.9  $\mu\text{m}$  bands with the 7.7  $\mu\text{m}$  feature supports their assignment to the UIR spectrum.

Figure 10 and Table 5 also contain information on the ranges of variations actually observed in band strengths. These deviations greatly exceed the error bars in Figures 3–9; they

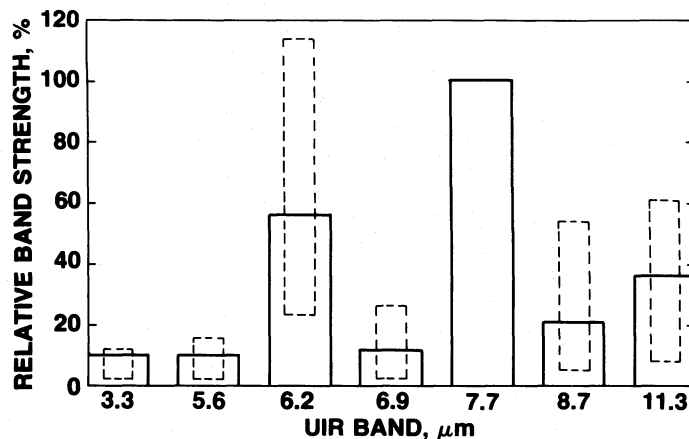


FIG. 10.—“Generic spectrum” of UIR features. Solid lines represent the average band strengths, relative to 100% for that at 7.7  $\mu\text{m}$ , defined from the intercepts in Table 4. Dashed rectangles represent the observed ranges of feature strengths that we have observed.

TABLE 5  
BAND STRENGTHS IN THE "GENERIC" UIR SPECTRUM [RELATIVE TO  $I(7.7 \mu\text{m})$ ]

PARAMETER	UIR BAND ( $\mu\text{m}$ )						
	3.3	5.6	6.2	6.9	7.7	8.7	11.3
Average .....	0.10	0.10	0.56	0.12	1.00	0.21	0.36
Observed Range .....	0.02–0.12	0.02–0.16	0.23–1.14	0.02–0.26		0.05–0.54	0.08–0.61

are, therefore, real. To emphasize the sometimes substantial variations that occur, we have plotted the upper limits for the 5.6 and 6.9  $\mu\text{m}$  features in HD 44179 in Figures 4, 5, 6, and 9. In some objects, there is also a broad hump that underlies both the 6.2 and the 7.7  $\mu\text{m}$  features (see § III; Bregman *et al.* 1985; Russell, Soifer, and Willner 1977; Sellgren *et al.* 1985). In contrast, HD 44179 shows no evidence for such a feature.

#### V. THE DEPENDENCE ON CARBON

In Figure 11 we demonstrate the role of nebular, gas-phase carbon richness on the UIR features in planetary nebulae. The ordinate represents the fraction of integrated far-infrared luminosity that a nebula radiates in its 7.7  $\mu\text{m}$  band, " $f(7.7 \mu\text{m})$ ". Far-infrared luminosity is assessed from the *IRAS* data on these nebulae and represents the flux integrated between 7 and 140  $\mu\text{m}$  (between *IRAS* band 1 and 4). The abscissa is the C/O ratio determined from ultraviolet observations, with the single exception of IC 5117 whose C/H has been determined solely from the C II  $\lambda 4267$  line (Aller and Czyzak 1983; Shields 1978; Perinotto, Panagia, and Benvenuti 1980; Torres-Peimbert and Pena 1981; Adams and Seaton 1982; Flower and Penn 1981).

In spite of the paucity of nebulae that can be plotted in Figure 11 at present, it is clear that increasing nebular C/O correlates well with the increasing importance of the fraction of infrared luminosity emitted in the UIR spectrum (as epitomized by the strongest band, at 7.7  $\mu\text{m}$ ). It is also clear, from Figures 3–9, that similar trends must exist between C/O and the fractional luminosities of other UIR bands. We also find good correlations between  $f(7.7 \mu\text{m})$  and both C/H and

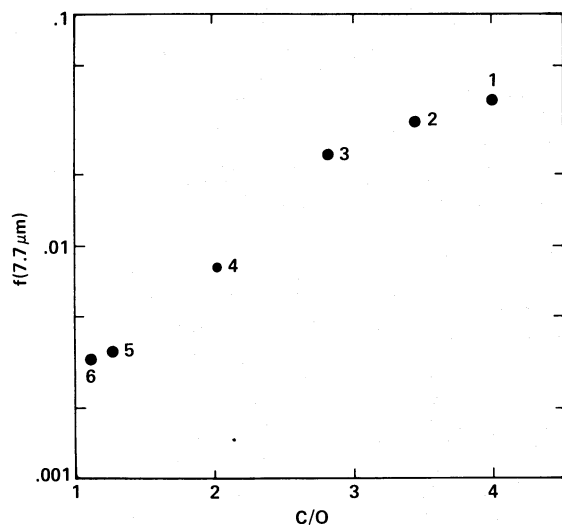


FIG. 11.—The correlation between  $f(7.7 \mu\text{m})$ —the fraction of nebular far-infrared luminosity radiated by the 7.7  $\mu\text{m}$  band—and nebular C/O ratio. Key: 1, J900; 2, NGC 7027; 3, BD +30°3639; 4, IC 5117; 5, IC 418; 6, NGC 6572.

(C—O)/H for five of the six planetaries plotted in Figure 11. However, in each of these other correlations, BD +30°3639 falls far from the locus defined by the other nebulae. Only the trend shown by Figure 11 accommodates all six planetaries. We find no correlations between the UIR features and either nebular electron density, or far-infrared luminosity, or nuclear effective temperature for the planetaries.

#### VI. DISCUSSION

##### a) Spectral Variation

The correlations shown in Figures 3–9 indicate that all the various UIR features go together. This renders the concept of a generic UIR spectrum (Table 5) a valid one. This general correlation strongly suggests that a single class of chemical species is the carrier of the UIR bands. It rules out, therefore, the model based upon fluorescence from many different types of molecules in an "icy" grain mantle (Allamandola, Greenberg, and Norman 1979).

Despite the presence of an overall generic spectrum, there are real variations in the relative strengths of the UIR bands in different objects. In principle, these variations may provide a good clue to the identification of the specific PAH species responsible for the emission. Such an identification, however, has to await laboratory data on partially hydrogenated, ionized PAHs in both ground and electronically excited states.

The observed variations in relative strength of the UIR bands from object to object could be caused by either of two mechanisms. First, it might be due to excitation effects. When the average vibrational energy available per mode increases, the relative intensity increases faster for the high-frequency modes than for the low-frequency ones. (The number of normal modes of vibration per PAH molecule is given by  $3N - 6$ , where  $N$  is the number of atoms in the molecule.) This effect is particularly important for the ratio of the 3.3 to the 11.3  $\mu\text{m}$  modes (Allamandola, Tielens, and Barker 1985a, b). Such variations in the average excitation energy could be caused by variations in the UV photon field that excites the molecules.

The second mechanism that can produce variations in the relative strengths of the UIR bands among different objects is, of course, compositional variations in the collection of PAHs present in different objects. Such variations are probably responsible for the changes in relative band strength, frequency of the peak, and shape of the 7.7  $\mu\text{m}$  band, which is presumed to be caused by a collection of overlapping C—C stretching modes in different molecules. More importantly, however, compositional variations in the collection of PAHs between different objects may cause variations in the average number of carbon atoms per molecule and, therefore, in the average excitation energy per normal mode upon absorption of a typical UV photon. This effect is similar to that caused by changes in the average UV photon excitation energy of the PAHs in dif-

TABLE 6  
RATIOS OF 11.3 MICRON TO 3.3 MICRON BANDS FOR DIFFERENT SOURCES

Object	$I(11.3)/I(3.3)$	Vibrational Energy <sup>a</sup> (cm <sup>-1</sup> )	Number of C atoms <sup>b</sup>
IC 418.....	4.6	26,400	51
J900.....	2.0	43,000	29
M1-11.....	4.2	27,000	49
NGC 6572.....	3.1	< 30,000	40
BD + 30°3639.....	2.7	36,000	36
NGC 7027.....	5.3	25,200	56
IC 5117.....	4.7	26,400	52
HD 44179.....	2.0	43,000	29
GL 437.....	8.7	20,500	78
Orion Bar.....	3.0	31,000	39
	4.5	26,300	50
	3.1	30,000	40
	4.0	27,600	48
	3.1	30,000	40
	3.4	29,000	42
	2.8	37,000	37
M1-78.....	3.0	31,000	39

<sup>a</sup> Assuming a PAH with 40 carbon atoms (see text, § VIa).

<sup>b</sup> Assuming a PAH containing 30,000 cm<sup>-1</sup> of vibrational energy (see text, § VIa).

ferent sources, and it will be difficult to distinguish between these two mechanisms.

In Table 6 we have analyzed the 3.3 and 11.3  $\mu\text{m}$  data in terms of these two mechanisms (Allamandola, Tielens, and Barker 1985b). First, assuming a vibrational excitation energy of 30,000 cm<sup>-1</sup>, the average number of carbon atoms is calculated from the ratio of 11.3 to 3.3  $\mu\text{m}$  bands observed in each source. (Implicit in this analysis is the assumption that the smallest PAHs are the brightest and therefore dominate the spectrum.) Second, assuming an average number of 40 carbon atoms per molecule, the vibrational excitation energy is calculated. Note that the average vibrational excitation energy is probably much less than the energy of the absorbed UV photon, because the PAH is probably electronically excited as well, and because the observed intensities in the UIR bands are an average over the relaxation cascade in a given PAH (Allamandola, Tielens, and Barker 1985b).

In a few particular cases it is possible to identify which of these two mechanisms dominates. Compare, for example, the ratios of the 11.3 to 3.3  $\mu\text{m}$  bands for NGC 7027 and HD 44179. The ratio is actually lower for the cooler object (HD 44179), contrary to what would be expected if the variation in the UV photon excitation energy were to cause the variation in band ratio. It is, therefore, likely that HD 44179 has a different collection of PAHs responsible for its emission bands than NGC 7027 has. A difference in the collections of emitting PAHs is also supported by a detailed examination of the infrared spectra of these sources. In particular, HD 44179 does not show the broad hump underlying the 6.2 and 7.7  $\mu\text{m}$  bands. Nor does it show the broad, weak near-infrared plateau of emission between 3.25 and 3.6  $\mu\text{m}$  (Geballe *et al.* 1985). Most other nebulae display both of these broader components. Possibly small PAHs survive in the benign conditions around HD 44179 while they are destroyed in the harsh environment of NGC 7027. Since the smallest PAHs with relatively few modes produce the brighter mid-infrared emission bands, they would dominate the spectrum of HD 44179, leading to a "simple"

spectrum in this object. The broad hump underneath the 6.2 and 7.7  $\mu\text{m}$  features and the emission plateau between 3.25 and 3.6  $\mu\text{m}$  are then presumably due to a forest of overlapping lines arising from a mixture of larger PAHs producing a pseudocontinuum.

Another good example of compositional variation is provided by the ratio of the 6.2 and 7.7  $\mu\text{m}$  bands. These bands are so close in energy that differences in the average excitation energy per mode in the emitting molecules do not influence their ratio very much (Allamandola, Tielens, and Barker 1985b). Typically  $I(6.2)/I(7.7)$  is about 0.5. However, IC 5117 and P18, for example, show ratios close to unity, while NGC 7027 and NGC 6572 have ratios of 0.23 and < 0.20, respectively. This, too, is consistent with smaller PAHs being more important than larger ones and dominating the spectrum in the objects with less intense UV fields. Similar variations occur for the other bands in the 5–8  $\mu\text{m}$  region.

#### b) The Correlation with the C/O Abundance Ratio

The correlation of the ratio of the 7.7  $\mu\text{m}$  UIR emission to the far-infrared dust emission with the nebular C/O ratio for planetaries provides general support for an origin of the UIR bands in carbonaceous material, such as PAHs. This correlation may yield insights into the process of carbon condensation in planetary nebulae because it is likely that PAHs are the molecular precursors of carbon dust grains (Crawford, Tielens, and Allamandola 1985).

The observed ratio of 7.7  $\mu\text{m}$  flux to far-infrared flux essentially measures the far-ultraviolet absorption cross section of the PAHs with respect to that of the larger carbon dust grains in planetaries. The correlation with C/O might, for example, be due to less complete condensation of carbon grains for higher C/O ratios, so that relatively more carbon is trapped in PAH species. Alternatively, it may be due to particle growth effects. The higher the value of the C/O ratio, the larger the carbon dust particles grow. The ultraviolet cross section of carbon grains per unit volume goes down when particle size increases, so relatively more ultraviolet photons are absorbed by PAHs, leading to an increase in  $L(7.7 \mu\text{m})/L(\text{FIR})$ .

#### c) Other Carbon-rich Stars

The present study, by keeping constant the class of object to planetaries, in which the emitting species are produced, clearly shows the importance of carbon richness in an ultraviolet-rich nebular environment. Carbon and ultraviolet are not sufficient conditions, however, as other dusty carbon-rich objects do not show the bands. Neither extreme carbon stars such as IRC + 10216, nor carbon-rich nebulae such as GL 2688, nor the dusty Population I WC9 Wolf-Rayets have UIR features. The absence in carbon-rich Miras and GL 2688 is probably due to the absence of UV photons. The WC9 stars, by contrast, are very hot. The absence of UIR bands in these objects suggests that other physical or chemical properties of carbon-rich outflows are important in producing emission from PAHs. For example, the infrared excesses in the WC9 stars mimic blackbody curves over a wide wavelength range (e.g., Cohen, Barlow, and Kuhl 1975; Cohen 1975; Gehrz and Hackwell 1974) yet the dust shells of the WC9's are optically very thin at near-infrared wavelengths (Allen, Barton, and Wallace 1981). This may indicate that the circumstellar carbon-rich grains are quite large, suppressing any spectral signatures. Perhaps condensation in the WC9 stars takes place much more rapidly and

completely than in planetaries, so that all PAHs have been incorporated into dust particles. Certainly the comparison between Population I WC9 stars and the WC10 planetary nebular nuclei is a crucial one, for their circumstellar properties are very similar, yet these WC10 objects reveal UIR bands in their spectra (Aitken *et al.* 1980) whereas the Population I Wolf-Rayets do not.

We thank the staff and management of the KAO for their assistance with, and support of, our airborne observations. Martin Cohen thanks NASA for support during this study under its Airborne Astronomy Program. A. G. G. M. Tielens acknowledges support through NASA grant NCA2-1R050-405. We thank an anonymous referee for many useful suggestions.

## REFERENCES

- Acker, A. 1978, *Astr. Ap. Suppl.*, **33**, 367.  
 Adams, S., and Seaton, M. J. 1982, *M.N.R.A.S.*, **200**, 7P.  
 Aitken, D. K. 1981, in *IAU Symposium 96, Infrared Astronomy*, ed. C. G. Wynn-Williams and D. P. Cruikshank (Dordrecht: Reidel), p. 207.  
 Aitken, D. K., Barlow, M. J., Roche, P. F., and Spencer, P. M. 1980, *M.N.R.A.S.*, **192**, 679.  
 Aitken, D. K., and Roche, P. F. 1982, *M.N.R.A.S.*, **200**, 217.  
 ———, 1984, *M.N.R.A.S.*, **208**, 751.  
 Aitken, D. K., Roche, P. F., Spenser, P. M., and Jones, B. 1979, *Ap. J.*, **233**, 925.  
 Allamandola, L. J., Greenberg, J. M., and Norman, C. A. 1979, *Astr. Ap.*, **77**, 66.  
 Allamandola, L. J., Tielens, A. G. G. M., and Barker, J. R. 1985a, *Ap. J. (Letters)*, **290**, L25.  
 ———, 1985b, in preparation.  
 Allen, D. A., Baines, D. W. T., Blades, J. C., and Whittet, D. C. B. 1982, *M.N.R.A.S.*, **199**, 1017.  
 Allen, D. A., Barton, J. R., and Wallace, P. T. 1981, *M.N.R.A.S.*, **196**, 797.  
 Aller, L. H., and Czyzak, S. J. 1983, *Ap. J. Suppl.*, **51**, 211.  
 Barlow, M. J. 1983, in *IAU Symposium 103, Planetary Nebulae*, ed. D. R. Flower (Dordrecht: Reidel), p. 105.  
 Becklin, E. E., Beckwith, S., Gatley, I., Matthews, K., Neugebauer, G., Sarazin, C., and Werner, M. W. 1976, *Ap. J.*, **207**, 770.  
 Bregman, J. D., Allamandola, L. J., Geballe, T. R., Tielens, A. G. G. M., and Witteborn, F. C. 1985, in preparation.  
 Bregman, J. D., Dinerstein, H. L., Goebel, J. H., Lester, D. E., Witteborn, F. C., and Rank, D. M. 1983, *Ap. J.*, **274**, 666.  
 Cohen, M. 1975, *M.N.R.A.S.*, **173**, 489.  
 Cohen, M., and Barlow, M. J. 1980, *Ap. J.*, **238**, 585.  
 Cohen, M., Barlow, M. J., and Kuhl, L. V. 1975, *Astr. Ap.*, **40**, 291.  
 Crawford, M. K., Tielens, A. G. G. M., and Allamandola, L. J. 1985, *Ap. J. (Letters)*, **293**, L45.  
 Duley, W. W., and Williams, D. A. 1981, *M.N.R.A.S.*, **196**, 269.  
 Dwek, E., Sellgren, K., Soifer, B. T., and Werner, M. W. 1980, *Ap. J.*, **238**, 140.  
 Flower, D. R., and Penn, C. J. 1981, *M.N.R.A.S.*, **194**, 13P.  
 Geballe, T. R., Lacy, J. H., Persson, S. E., McGregor, P. J., and Soifer, B. T. 1985, *Ap. J.*, **292**, 500.  
 Gehrz, R. D., and Hackwell, J. 1974, *Ap. J.*, **194**, 619.  
 Kleinmann, S. G., Sargent, D. G., Gillett, F. C., Grasdalen, G. L., and Joyce, R. R. 1977, *Ap. J. (Letters)*, **215**, L79.  
 Leger, A., and Puget, J. L. 1984, *Astr. Ap.*, **137**, L5.  
 Perinotto, M., Panagia, N., and Benvenuti, P. 1980, *Astr. Ap.*, **85**, 332.  
 Pottasch, S. R. 1984, in *IAU Symposium 103, Planetary Nebulae* (Dordrecht: Reidel), p. 62.  
 Russell, R. W., Soifer, B. T., and Merrill, K. M. 1977, *Ap. J.*, **213**, 66.  
 Russell, R. W., Soifer, B. T., and Willner, S. P. 1977, *Ap. J. (Letters)*, **217**, L149.  
 ———, 1978, *Ap. J.*, **220**, 568.  
 Schmidt, G. D., Cohen, M., and Margon, B. 1980, *Ap. J. (Letters)*, **239**, L133.  
 Sellgren, K. 1984, *Ap. J.*, **277**, 623.  
 Sellgren, K., Allamandola, L. J., Bregman, J. D., Werner, M. W., and Wooden, D. H. 1985, *Ap. J.*, **299**, 416.  
 Sellgren, K., Werner, M. W., and Dinerstein, H. L. 1983, *Ap. J. (Letters)*, **271**, L13.  
 Shields, G. A. 1978, *Ap. J.*, **219**, 565.  
 Torres-Peimbert, S., and Pena, M. 1981, *Rev. Mexicana Astr. Ap.*, **6**, 301.  
 Wade, R. 1983, *Proc. Soc. Photo-Opt. Instrum. Eng.*, **445**, 47.  
 Whitcomb, S. E., Gatley, I., Hildebrand, R. H., Keene, J., Sellgren, K., and Werner, M. W. 1981, *Ap. J.*, **246**, 416.  
 Willner, S. P., Jones, B., Puetter, R. C., Russell, R. W., and Soifer, B. T. 1979, *Ap. J.*, **234**, 496.  
 Witt, A. N., Schild, R. E., and Kraiman, J. B. 1984, *Ap. J.*, **281**, 708.  
 Witteborn, F. C., and Bregman, J. D. 1984, *Proc. Soc. Photo-Opt. Instrum. Eng.*, **509**, 123.  
 Wynn-Williams, C. G., Becklin, E. E., Beichman, C. A., Capps, R. W., and Shakeshaft, J. R. 1981, *Ap. J.*, **246**, 801.

L. J. ALLAMANDOLA, J. BREGMAN, M. COHEN, J. SIMPSON, A. G. G. M. TIELENS, F. C. WITTEBORN, and D. WOODEN: NASA/Ames Research Center, Mailstop 245-6, Moffett Field, CA 94035

D. M. RANK: Lick Observatory, University of California, Santa Cruz, CA 95064